

Exploring connections between statistical mechanics and Green's functions for realistic systems. Temperature dependent entropy and internal energy from a self-consistent second-order Green's function.

Alicia Rae Welden,^{1,*} Alexander A. Rusakov,^{1,†} and Dominika Zgid^{1,‡}

¹*Department of Chemistry, University of Michigan, Ann Arbor, Michigan 48109, USA*

Including finite-temperature effects into electronic structure calculations of semiconductors and metals is frequently necessary, but can become cumbersome using zero-temperature methods, which require an explicit evaluation of excited states to extend the approach to finite-temperature. Using a Matsubara Green's function formalism, it is easy to include the effects of temperature and to connect dynamic quantities such as the self-energy with static thermodynamic quantities such as the Helmholtz energy, entropy, and internal energy. We evaluate the thermodynamic quantities with a self-consistent Green's function where the self-energy is approximated to second-order (GF2). To validate our method, we benchmark it against finite temperature full configuration interaction (FCI) calculations for a hydrogen fluoride (HF) molecule and find excellent agreement at high temperatures and very good agreement at low temperatures. Then, we proceed to evaluate thermodynamic quantities for a one-dimension hydrogen solid at various interatomic separations and temperatures. At many points in the phase diagram of this system, multiple phases such as a metal and an insulator exist, and we are able to determine the most stable phase from the Helmholtz energy. Overall, this machinery provides a method to calculate temperature dependent electronic structure and thermodynamic quantities to determine phase stability for materials where temperature effects are important.

I. INTRODUCTION

In molecular quantum-chemical calculations of thermodynamic properties such as Gibbs energy^{1,2}, the temperature dependent component is usually dominated by vibrational contributions. This is due to the large gaps between electronic states, which ensures that the excited state populations will be negligible. Consequently, common molecular calculations do not explicitly include temperature effects on the electronic structure.

However, for materials such as doped semiconductors³ the magnitude of the electronic band gap can be relatively small, or for metals nonexistent altogether, allowing electronic states other than the ground state to be accessible at low temperatures. Thus, it is necessary to include temperature effects into the electronic description. Even though for most materials the vibrational contribution to the specific heat is much larger than the electronic one, there are cases when the incorporation of the electronic contribution is necessary. The electronic contribution to specific heat is important for **(i)** heavy fermion materials at low temperatures⁴, **(ii)** materials that do not undergo a structural transition that changes the vibrational contribution, causing the stability of phases to primarily depend on the relative electronic contribution to Gibbs energy, **(iii)** materials with a structural transition where the difference between vibrational contributions of the phases is of the same order as the difference between electronic contributions^{5,6}. Thus, modern materials calculations can benefit from computational tools that provide access to the temperature dependent electronic contribution to the specific heat, Gibbs energy, entropy, or electronic part of the partition function.

While in traditional quantum chemical calculations

evaluating the electronic contribution to temperature dependent quantities is certainly not wide spread, a number of such methods exist, most notably, the finite temperature Hartree-Fock (HF)⁷, density functional theory (DFT)⁸⁻¹¹, Møller-Plesset second order perturbation theory (MP2)¹², coupled-cluster (CC)¹³⁻¹⁵, and Lanczos method^{16,17} for finite temperature configuration interaction calculations. However, these methods are usually quite difficult to implement and costly to use since they rely on the modification of the parent zero-temperature method to the finite temperature formalism by adapting it to work in the canonical or grand canonical ensemble. For example to carry out such calculations in the CI formalism, one must obtain the excited states and corresponding Boltzmann factors in order to evaluate the partition function and thermodynamic averages, making application of finite temperature variants of these methods quite cumbersome.

Conversely, for the Green's function formalism the connection to thermodynamics arises in a straightforward manner and was derived in numerous books in the past¹⁸⁻²¹. While this connection is well understood from the theoretical view point, the actual numerical calculations of the desired quantities still remain quite challenging. This is because in order to gain access to thermodynamic quantities a full self-consistent calculation of the imaginary axis (Matsubara) Green's function is desired (the non-self-consistent Green's function can yield non-unique thermodynamic quantities). These calculations are difficult for multiple reasons, such as large imaginary time and frequency grids, multiple solutions of non-linear equations that can be present, etc. This is why in the recent years, calculations that capitalized on Green's function language and yield thermodynamic quantities where mostly done for model systems²²⁻²⁶. Currently, there are

only a few research groups that have managed to rigorously generalize the finite temperature Green's function formalism to deal with a general Hamiltonian containing all the realistic interactions.

To the best of our knowledge, here, we present the first application of the fully self-consistent finite temperature Green's function formalism to evaluate thermodynamic quantities and phase stability for a periodic system described by a full quantum chemistry Hamiltonian. We demonstrate that Green's function formalism leads to a simple calculation of the electronic contribution to the Helmholtz/Gibbs energy, entropy, grand potential, and partition function without explicitly performing any excited state calculations. The presented formalism is exact at the infinite temperature limit since the perturbative Green's function formulation is a perturbation that contains the inverse temperature as small parameter.

This paper is organized as follows. In Sec. II, we introduce the imaginary Green's function formalism and familiarize the readers with its connection to thermodynamics. In Sec. III, we list properties of the Luttinger-Ward functional which is our main computational object and we explain its evaluation within a self-consistent Green's function second-order (GF2) periodic implementation in Sec. IV. We present numerical results for a simple molecular problem to benchmark our method and we progress to a periodic system to discuss the phase stability and phase diagram for a one-dimensional hydrogen solid in Sec. V. Finally, we form conclusions in Sec. VI.

II. CONNECTION WITH THERMODYNAMICS

One of the first descriptions of the connection between the Green's function formalism and thermodynamics was presented in the book by Abrikosov, Gorkov, and Dzyaloshinski²¹. Since then multiple texts appeared that discuss such a connection^{18,20,27}. For an excellent, detailed derivation, we encourage the reader to follow Ref. 18; here, we will only mention few basic Green's function equations for the sake of completeness.

The one-body Green's function is defined as

$$G_{ji}(z_1, z_2) \equiv \frac{\text{Tr}[e^{-\beta\hat{H}^M} \hat{G}_{ji}(z_1, z_2)]}{\text{Tr}[e^{-\beta\hat{H}^M}]} \quad (1)$$

$$= \frac{1}{i} \frac{\text{Tr}[\tau \{e^{-i \int_{\gamma} d\bar{z} \hat{H}(\bar{z})} \hat{d}_{j,H}(z_1) \hat{d}_{i,H}^{\dagger}(z_2)\}]}{\text{Tr}[\tau \{e^{-i \int_{\gamma} d\bar{z} \hat{H}(\bar{z})}\}]} ,$$

where $\hat{d}_{j,H}(z_1)$ and $\hat{d}_{i,H}^{\dagger}(z_2)$ are the second-quantized annihilation and creation operators in the Heisenberg representations and $\beta = 1/(k_B T)$ is the inverse temperature while T is the actual temperature and k_B is the Boltzmann constant. This Green's function, depending on how the contour γ in the complex plane is closed, can be used to describe system's time evolution (when z_1 and z_2 are set to the real-time variables), zero temperature phenomena, or equilibrium phenomena at finite temperature.

Here, we are interested in a formalism used to calculate

the initial ensemble average that is applied to systems in thermodynamic equilibrium at finite temperature. This approach is called Matsubara formalism or the "finite-temperature formalism". For this reason, in the Green's function from Eq. 1 we set $z_1 = t_0 - i\tau_1$ and $z_2 = t_0 - i\tau_2$. Consequently, the Green's function

$$G_{ji}^M(\tau_1, \tau_2) = \frac{1}{i} \left\{ \theta(\tau_1 - \tau_2) \frac{\text{Tr}[e^{(\tau_1 - \tau_2 - \beta)\hat{H}^M} \hat{d}_j e^{(\tau_2 - \tau_1)\hat{H}^M} \hat{d}_i^{\dagger}]}{\text{Tr}[e^{-\beta\hat{H}^M}]} \right. \\ \left. \pm \theta(\tau_2 - \tau_1) \frac{\text{Tr}[e^{(\tau_2 - \tau_1 - \beta)\hat{H}^M} \hat{d}_i^{\dagger} e^{(\tau_1 - \tau_2)\hat{H}^M} \hat{d}_j]}{\text{Tr}[e^{-\beta\hat{H}^M}]} \right\} \quad (2)$$

does not describe any time evolution of the system under study. Instead, in this Green's function the initial state of the system can be the thermodynamic state corresponding to a Hamiltonian, $\hat{H}^M = \hat{H}(t_0) - \mu\hat{N}$, where \hat{N} is the particle number operator. Thus, from such a defined Matsubara Green's function, the initial ensemble average of any one-body operator $\hat{O} = \sum_{ij} O_{ij} \hat{d}_i^{\dagger} \hat{d}_j$, can be evaluated simply as

$$O = \frac{\text{Tr}[e^{-\beta\hat{H}^M} \hat{O}]}{\text{Tr}[e^{-\beta\hat{H}^M}]} = \pm i \sum_{ij} O_{ij} G_{ji}^M(\tau), \quad (3)$$

where $\tau = \tau_1 - \tau_2$ since the one-body Green's function matrix elements depend only on the difference of the imaginary time variables. Furthermore, the imaginary time Green's function $G(\tau)$ can be Fourier transformed to the imaginary frequency Green's function $G(i\omega_n)$ where for fermions the frequency grid is given by $\omega_n = \frac{(2n+1)\pi}{\beta}$ with n defined here as a positive integer. For simplicity, in the remainder of this paper, we will drop subscript M denoting Matsubara Green's functions since from now on we will only discuss this finite temperature formalism.

The discussion above shows that at finite temperature one can get grand canonical ensemble averages of one-body operators using the Matsubara formalism. However, let us ask one more question: Can we get a system's static thermodynamic variables such as electronic Gibbs or Helmholtz energy, internal energy, and electronic entropy from dynamic (frequency dependent) variables such as Green's function and self-energy?

The thermodynamics of a system can be described by a thermodynamical potential, such as the grand potential Ω ¹⁸

$$\Omega = \frac{1}{\beta} \{ \Phi - \text{Tr}[\Sigma G + \ln(\Sigma - G_0^{-1})] \}, \quad (4)$$

where the self-energy $\Sigma = \Sigma(i\omega_n)$ describes all the correlational effects present in the system and $G_0 = G_0(i\omega_n)$ is the reference (usually non-interacting) system's Green's function and $G = G(i\omega_n)$ is the interacting Green's function. The interacting and non-interacting Green's functions are connected through the Dyson equation, $\Sigma = G_0^{-1} - G^{-1}$. The Φ functional from Eq. 4 is called

the Luttinger-Ward functional²⁸ and is defined as

$$\Phi = \sum_{m=1}^{\infty} \frac{1}{2m} \text{Tr} \left[\sum_n \Sigma^{(m)}(i\omega_n) G(i\omega_n) \right], \quad (5)$$

where $\Sigma^{(m)}(i\omega_n)$ is a self-energy containing all irreducible and topologically inequivalent diagrams of order m . The detailed derivation of Eq. 4 is presented in Ref. 18. Note that in some texts the functional Φ is simply referred to as the Phi functional and the functional Ω is called the Luttinger-Ward functional.

Thus, the computational object that provides a connection between the static and dynamic quantities is the Luttinger-Ward functional. This scalar functional $\Phi = \hat{\Phi}[G]$ depends on the Green's function and has multiple important properties for Green's function theory.

III. PROPERTIES OF THE LUTTINGER-WARD FUNCTIONAL

The formal properties of Luttinger-Ward functional have been discussed extensively before. The functional has previously been applied to calculate energies for atoms and molecules^{29,30}, the electron gas³¹, as well as for the Hubbard lattice^{23,24,32,33}. In the following section, we will only outline some of the most salient properties of the Luttinger-Ward functional that can benefit the reader.

A. Self-energy as a functional derivative

The self-energy $\Sigma = \Sigma(i\omega_n)$ can be obtained as a functional derivative of the Luttinger-Ward functional

$$\beta \frac{\delta \hat{\Phi}[G]}{\delta G} = \hat{\Sigma}[G]. \quad (6)$$

Here, the self-energy is defined as a functional of Green's function that is evaluated independent of the Dyson equation. Consequently, in the non-interacting limit, where $\Sigma = 0$, it follows that the Luttinger-Ward functional is zero itself, $\hat{\Phi}[G] = 0$.

B. Connection with the grand potential Ω

The grand potential is a number but the mathematical object defined in Eq. 4 can be viewed more generally as a functional of Green's functions $\Omega[G]$. When a Green's function is a self-consistent solution of the Dyson equation then the variational derivative $\frac{\delta \Omega[G]}{\delta G} = 0$ since $\delta \Phi = \text{Tr}[\Sigma \delta G]$ and $\delta \Omega[G] = \frac{1}{\beta} \{ \delta \Phi - \text{Tr}[\delta \Sigma G + \Sigma \delta G - G \delta \Sigma] \}$. Consequently, we can conclude that the functional $\Omega[G]$ at the stationary point is equal to the grand potential.

Having grand potential one gains access to the partition function (Z) since

$$\Omega = -\frac{1}{\beta} \ln Z. \quad (7)$$

The Helmholtz energy, $A = E - TS$, where E is the internal energy and S is the entropy of a system at a given temperature T is connected to the grand potential as $A = \Omega + \mu N$, where N is the number of electrons in the system. Thus, knowing grand potential, we can easily calculate the electronic entropy as

$$S = \frac{E - \Omega - \mu N}{T} \quad (8)$$

as long as we have access to the internal energy of a system. The internal energy at a given temperature T can be evaluated using the Galitskii-Migdal formula

$$E = \frac{1}{2} \text{Tr} [(h + F) \gamma] + \frac{2}{\beta} \sum_n^{N_\omega} \text{Re}(\text{Tr}[G(i\omega_n) \Sigma(i\omega_n)]), \quad (9)$$

where γ is the one-body density matrix, h is the one-body Hamiltonian, F is the Fock matrix of a system, and N_ω is the size of the imaginary grid. Consequently, having access to the Luttinger-Ward functional of a system yields multiple electronic thermodynamic quantities.

C. Universality

Given two systems A and B at the same physical temperature T and the same chemical potential μ described by two Hamiltonians $\hat{H}_A = \sum_{ij} t_{ij}^A a_i^\dagger a_j + \sum_{ijkl} v_{ijkl} a_i^\dagger a_j^\dagger a_l a_k$ and $\hat{H}_B = \sum_{ij} t_{ij}^B a_i^\dagger a_j + \sum_{ijkl} v_{ijkl} a_i^\dagger a_j^\dagger a_l a_k$ such that they have the same two-body integrals v_{ijkl} but different one-body integrals $t^A \neq t^B$ the Luttinger-Ward functional is same (universal) for both of them. Since $\hat{\Phi}^A = \hat{\Phi}^B$, then it must also hold that $\hat{\Sigma}^A(G) = \hat{\Sigma}^B(G)$. In other words, two systems described by different G_0 but having the same two-body interactions are described by the same Luttinger-Ward functional.

IV. EVALUATION OF LUTTINGER-WARD FUNCTIONAL WITHIN GF2

A. Description of the GF2 algorithm

The Green's function and self-energy we evaluate in this work are computed using a perturbative method where the self-energy is self-consistently evaluated at the second-order (GF2) level. GF2 is advantageous for many reasons, namely, among others it behaves qualitatively correct for some strongly correlated systems³⁴, unlike methods such as MP2 or CCSD which tend to diverge

in these cases. GF2 has small fractional charge and fractional spin errors³⁵. GF2 is carried out self-consistently on imaginary time τ and imaginary frequency $i\omega_n$ axes with a computational scaling of $\mathcal{O}(n_\tau N^5)$ for molecular cases, where n_τ is a prefactor that depends on the size of the imaginary time grid and N is the number of orbitals present in the problem. We build the Green's function using the following expression

$$G(i\omega_n) = [(i\omega_n + \mu)S - F - \Sigma(i\omega_n)]^{-1} \quad (10)$$

where F and S are the Fock and overlap matrices in the atomic orbital (AO) basis, respectively, and μ is the chemical potential, which guarantees a correct particle number. To obtain $\Sigma(i\omega_n)$, we solve the Dyson equation given as

$$\Sigma(i\omega_n) = G_0(i\omega_n)^{-1} - G(i\omega_n)^{-1} \quad (11)$$

where $G_0(i\omega_n) = [(i\omega_n + \mu)S - F]^{-1}$ is the non-interacting Green's function while $G(i\omega_n)$ is the interacting Green's function since it contains the self-energy. To reduce scaling with the grid, we employ a spline interpolation method to evaluate the Green's function³⁶ and Legendre orthogonal polynomials to expand the $\Sigma(\tau)$ matrix³⁷. As pointed out previously, this self-consistent evaluation guarantees that both the Galitskii-Migdal and Luttinger-Ward energies are stationary with respect to the Green's function. For a full discussion of the algorithm and implementation details of GF2, we refer the reader to Refs. 34 and 35. The main computational object in our evaluation is the self-energy in the AO basis, which can be expressed as

$$\begin{aligned} \Sigma_{ij}(\tau) = & - \sum_{klmnpq} G_{kl}(\tau) G_{mn}(\tau) G_{pq}(\tau) \times \\ & \times v_{ikmq}(2v_{ljpn} - v_{pjln}). \end{aligned} \quad (12)$$

where v_{ijkl} are the two-electron integrals in the AO basis in the chemist's notation. This quantity is evaluated in a Legendre polynomial basis³⁷ to accelerate the calculation.

The details of periodic GF2 implementation have been reported in Ref.³⁸. The basic differences from the molecular version include solving the Dyson equation in \mathbf{k} -space via

$$G^k(i\omega_n) = [(i\omega_n + \mu)S^k - F^k - \Sigma^k(i\omega_n)]^{-1} \quad (13)$$

and complicating the real-space self-energy, $\Sigma^{\mathbf{0}\mathbf{g}}(\tau)$, evaluation by additional cell index summations:

$$\begin{aligned} \Sigma_{ij}^{\mathbf{0}\mathbf{g}}(\tau) = & - \sum_{\mathbf{g}_1, \dots, \mathbf{g}_6} \sum_{klmnpq} G_{kl}^{\mathbf{g}_3 \mathbf{g}_6}(\tau) G_{mn}^{\mathbf{g}_1 \mathbf{g}_4}(\tau) G_{pq}^{\mathbf{g}_5 \mathbf{g}_2}(-\tau) \times \\ & \times v_{imq}^{\mathbf{0}\mathbf{g}_1 \mathbf{g}_2 \mathbf{g}_3} (2v_{jnp}^{\mathbf{g}_4 \mathbf{g}_5 \mathbf{g}_6} - v_{jlpn}^{\mathbf{g}_6 \mathbf{g}_5 \mathbf{g}_4}). \end{aligned} \quad (14)$$

$\Sigma^k(i\omega_n)$ in Eq. 13 and $\Sigma^{\mathbf{0}\mathbf{g}}(\tau)$ in Eq. 14 are intercon-

vertible via corresponding Fourier transforms from the \mathbf{k} - to real-space and between the imaginary time and imaginary frequency domains also via Fourier transform. The self-energy calculation according to Eq. 14 results in $\mathcal{O}(N^5 N_{cell}^4 n_\tau)$ formal scaling of the computation cost with N the number of orbitals in the unit cell and N_{cell} the number of real space cells. This is typically a bottleneck of the GF2 self-consistency procedure.

The expression for the total energy likewise acquires a cell summation according to Eqs. 13 and 14 in Ref.³⁸:

$$\begin{aligned} E_{tot} = & E_{1b} + E_{2b} \\ = & \frac{1}{2} \sum_{\mathbf{g}, i, j} \gamma_{ij}^{\mathbf{0}\mathbf{g}} (2h_{ij}^{\mathbf{0}\mathbf{g}} + [\Sigma_\infty]_{ij}^{\mathbf{0}\mathbf{g}}) + \\ & + \frac{2}{\beta} \sum_{\mathbf{g}, i, j} \text{Re} \left[\sum_n G_{ij}^{\mathbf{0}\mathbf{g}}(i\omega_n) \Sigma_{ij}^{\mathbf{0}\mathbf{g}}(i\omega_n) \right]. \end{aligned} \quad (15)$$

B. Evaluation of the grand potential in the \mathbf{k} -space

The evaluation of the Luttinger-Ward functional in conserving approximations³⁹ such as the self-consistent second-order Green's function (GF2)^{34,35,37} is quite straightforward and was originally derived by Luttinger and Ward²⁸ as

$$\Phi^{(2)} = \frac{1}{4} \text{Tr} \left[\sum_n \Sigma^{(2)}(i\omega_n) G(i\omega_n) \right], \quad (16)$$

where $\Sigma^{(2)}(i\omega_n)$ is the frequency dependent part of the second-order self-energy. Since both $G(i\omega_n)$ and $\Sigma^{(2)}(i\omega_n)$ are readily available from a GF2 calculation, we are able to easily evaluate all terms of the functional.

The expression for grand potential from Eq. 4 can be conveniently reformulated as

$$\begin{aligned} \Omega_{LW} = & \frac{1}{2} \gamma \Sigma_\infty + \text{Tr}[G\Sigma] \\ & + \text{Tr}[\ln\{1 - G\Sigma\}] + \text{Tr}[\ln\{G_0^{-1}\}]. \end{aligned} \quad (17)$$

An excellent derivation of the above equation is given in Ref. 30 for molecular systems. However, as we mentioned before, for molecular systems the changes due to the electronic contributions of the Gibbs or Helmholtz energy are negligible due to the size of the gap. Here, we list detailed steps that need to be executed when dealing with crystalline systems where the electronic effects influencing Helmholtz energy can be significant.

In the periodic implementation, we evaluate the grand potential per unit cell, $\Omega^{\mathbf{0}\mathbf{0}}$. The overall expression is given as a sum of all the components

$$\begin{aligned} \Omega^{\mathbf{0}\mathbf{0}} = & \Omega_{\text{Tr}[G\Sigma]}^{\mathbf{0}\mathbf{0}} + \Omega_{\text{Tr}[\ln\{1-G\Sigma\}]}^{\mathbf{0}\mathbf{0}} \\ & + \Omega_{\text{Tr}[\ln\{G_0^{-1}\}]}^{\mathbf{0}\mathbf{0}} + \Omega_{\frac{1}{2}\gamma\Sigma_\infty}^{\mathbf{0}\mathbf{0}} \end{aligned} \quad (18)$$

where we sum the contribution per unit cell for each term present in Eq. 17. Due to the crystalline symmetry, it is

often more convenient to calculate these quantities in \mathbf{k} -space and transform the resulting quantity to the real space rather than using an explicit real space representation of all the quantities involved. All terms in Eq. 18 containing the Green's function G , or self-energy Σ were computed in \mathbf{k} -space and then Fourier transformed to real space. For example, to calculate the $\Omega_{\text{Tr}[G\Sigma]}^{00}$ contribution, we can first evaluate \mathbf{k} -dependent quantity

$$\Omega_{\text{Tr}[G\Sigma]}^k = \frac{2}{\beta} \sum_{i,j,n}^{N_\omega} G^k(i\omega_n)_{ij} \Sigma^k(i\omega_n)_{ji} \quad (19)$$

where the indices i and j run over all atomic orbitals in a given k -block. Subsequently, we perform Fourier transform of $\Omega_{\text{Tr}[G\Sigma]}^k$ to yield the real space $\Omega_{\text{Tr}[G\Sigma]}^{00}$ contribution.

The most cumbersome evaluation is of the term $\Omega_{\text{Tr}[\ln\{1-G\Sigma\}]}^{00}$, which requires diagonalization of the matrix $G^k \Sigma^k + (G^k \Sigma^k)^\dagger - G^k \Sigma^k (G^k \Sigma^k)^\dagger$, where the matrices G^k and Σ^k are understood to be dependent on $i\omega_n$. Once the eigenvalues of this matrix, ϵ_i^k , have been computed for each imaginary frequency point, $i\omega_n$, we have

$$\Omega_{\text{Tr}[\ln\{1-G\Sigma\}]}^k = \frac{2}{\beta} \sum_{n,i}^{N_\omega} \ln\{1 - \epsilon_i^k\}, \quad (20)$$

which can be Fourier transformed to the real space.

To include the contribution from the Fock matrix, $\Omega_{\text{Tr}[\ln\{G_0^{-1}\}]}^{00}$, we calculate

$$\Omega_{\text{Tr}[\ln\{G_0^{-1}\}]}^k = \begin{cases} \frac{1}{\beta} \sum_i \ln(1 + e^{\beta(\epsilon_i^k - \mu)}) + \epsilon_i^k, & \text{if } \epsilon_i^k - \mu < 0 \\ \frac{1}{\beta} \sum_i \ln(1 + e^{-\beta(\epsilon_i^k - \mu)}), & \text{otherwise.} \end{cases} \quad (21)$$

where by analyzing if the term $\epsilon_i^k - \mu$ is smaller or greater than zero we account for the cases where the absolute value of the Fock matrix eigenvalue can be large leading to numerical problems if only one branch of the above expression is used. This term accounts for occupation changes with temperature. For high β values (low values of the actual temperature T), the expression reduces to

$$\Omega_{\text{Tr}[\ln\{G_0^{-1}\}]}^k = \sum_{N_{occ}} \epsilon_i^k, \quad (22)$$

which allows electrons to occupy only the lowest available state, as is expected at a very low temperature.

We calculate the term $\Omega_{\frac{1}{2}\gamma\Sigma_\infty}^{00}$ directly in the real space as $\frac{1}{2}\gamma\Sigma_\infty$, since in the AO, the decay of both γ which is the density matrix and Σ_∞ which is the frequency independent part of the self-energy is rapid enough for a relatively few number of cells to assure a converged value of $\Omega_{\frac{1}{2}\gamma\Sigma_\infty}^{00}$.

V. RESULTS

A. HF molecule

In this section, we provide a calibration of the thermodynamic quantities such as internal energy E , grand potential Ω , entropy S , and chemical potential μ that are evaluated at the GF2 level and compared to the full configuration interaction (FCI) calculation. Since the evaluation of the thermodynamic quantities at the FCI level can be done only for very small molecular examples, we use here a hydrogen fluoride molecule (HF) since such a system has only 10 electrons and 6 basis functions in the STO-3G basis, resulting in a small number of possible configurations necessary to evaluate the FCI grand potential. Note that to describe a true physical system at very high temperature we would require a very large basis set. Here, we use HF as a model molecular system that is calculated in a minimal basis set solely to enable comparison of GF2 with FCI. The full configuration interaction (FCI) quantities for HF molecule were calculated previously by Kou and Hirata⁴⁰.

Let us first note that in order to calculate the FCI partition function and subsequently grand potential in the grand canonical ensemble, we need to evaluate

$$Z^{GC} = \sum_{N=0}^{2n} \sum_{S_z} \sum_i \langle \Phi_i^{(N,S_z)} | \exp\{-\beta(\hat{H} - \mu\hat{N})\} | \Phi_i^{(N,S_z)} \rangle, \quad (23)$$

where the $\Phi_i^{(N,S_z)}$ is the FCI wave function with N electrons and S_z quantum number and the number of possible occupation runs from 0 to $2n$, where n is the number of orbitals. Consequently, we need to explicitly get the information about every possible excited state present in the system with different number of electrons. Such a task quickly becomes impossible for any larger systems. In contrast, in Green's function methods, we never need to explicitly evaluate any information concerning specific excited states. It is sufficient to evaluate Eq. 17 and then Eq. 7 to obtain the grand canonical partition function. Thus, even for large systems such calculations remain feasible.

Results from our calibration are shown in Table I. For details about the parameters of the grid on which we evaluate can be found in⁴¹. In the high temperature limit, we are able to recover internal energy (E), grand potential (Ω) and entropy (S) in excellent agreement with FCI. Quantities at lower temperature show small deviation from the FCI results. While the temperature range in this example is huge, we would like to draw the reader's attention to the size of the HOMO-LUMO gap for this system, which is quite large. The Hartree-Fock gap for this system is ca. 1.0 a.u., corresponding to a temperature of around 3.0×10^5 K. Consequently, to make every state accessible to the electrons in this system, we require an extremely high temperature as indicated by our results.

T (K)	Internal Energy (a.u.)		Grand Potential (a.u.)		Entropy (k_B)		Chemical Potential (a.u.)	
	GF2	FCI	GF2	FCI	GF2	FCI	GF2	FCI
10^3	-98.588108	-98.596587	-95.521131	-99.844630	-0.002815	0.0	-0.000298	0.124804
10^4	-98.587920	-98.596583	-98.620717	-99.943772	0.000118	0.000113	0.003278	0.134719
10^5	-98.135409	-98.049385	-103.06678	-102.10659	3.566298	3.474720	0.380199	0.295683
10^6	-96.987785	-96.945339	-151.41037	-151.24440	4.949387	4.957688	3.874879	3.859897
10^7	-92.056939	-92.055572	-730.10020	-730.09520	5.347631	5.347656	46.86937	46.86892
10^8	-88.487425	-88.487404	-6847.0013	-6847.0025	5.405959	5.405959	504.6546	504.6548
10^9	-88.043269	-88.043292	-68126.725	-68126.811	5.406730	5.406727	5091.658	5091.666

TABLE I. FCI and GF2 results for HF molecule in STO-3G basis. A higher value of temperature corresponds to a smaller value of $\beta = 1/k_B T$

For our very lowest temperature (10^3 K), we recover a small negative entropy. This is a numerical artifact brought about from the level of convergence of the energies (1.0×10^{-5} a.u.) and the expression for entropy which requires multiplication by β . Thus, the smallest error $\approx 10^{-5}$ in energy will result in $\approx 10^{-3}$ error in entropy due to multiplication by $\beta = 100$ in the low temperature regime.

Overall, for this molecule, we were able to achieve a very good accuracy for the thermodynamic quantities involved using our GF2 method. While a FCI calculation requires computation of every state, we were able to produce the quantities of interest to reasonable accuracy using a single GF2 calculation at each temperature.

B. Periodic calculation of 1D Hydrogen

In our previous work, GF2 was implemented for periodic systems and applied to 1D hydrogen solid³⁸ in the mini-Huzinaga⁴² basis set. We consider the same system in this work, where we have used 5,000 Matsubara frequencies to discretize the Green's function in the frequency domain, 353 imaginary-time points, and 27 Legendre polynomials. We have found this grid size sufficient to evaluate energy differences between the systems. This system is simple enough to be a test bed for self-consistent Green's function theory; however, it displays a phase diagram that is characteristic of realistic solids. At different internuclear separations, corresponding to different pressures, we were able to recover multiple solutions. Although yielding different electronic energies and different spectra, these solutions can be mathematical artifacts of the nonlinear self-consistency procedure present in GF2; however, they can also have physical meaning corresponding to different solid phases. To decide which phase is more stable at a given temperature, it is necessary to consider the Helmholtz energies that we

are able to obtain from the Luttinger-Ward functional for each solution.

Previously, for the inverse temperature of $\beta = 100$, at most of the geometry points, we have identified two possible phases with different internal energies, E , that were obtained starting the iterative GF2 procedure either from an insulating or metallic solution. The results of our investigation can be found in Fig. 4 in Ref. 38. Currently, to analyze the stability of the solutions, for a range of inverse temperatures $\beta = 25, 75, 100$, we discuss internal energy E , Helmholtz energy A , and the entropic contribution TS to the Helmholtz energy. We also improved our convergence criteria not only converging the internal energy $E = E_{1b} + E_{2b}$ (as we have done in the previous work) but also converging both the E_{1b} , E_{2b} , and the Helmholtz energy separately. This much more stringent procedure to analyze convergence of GF2 leads us to slightly revised solutions for the 1D hydrogen solid which we discuss in the subsequent sections.

1. Short bond length/high pressure

At the interatomic separation of 0.75 \AA , we recovered only one gapless, metallic solution for all the values of inverse temperature ($\beta = 25, 75, 100$). We established that starting from two different initial guesses leads in both cases to two final solutions that were different in internal energy and Helmholtz energy by less than 10^{-4} a.u. Consequently, we deemed that we obtained the same metallic solution in both cases. The spectral functions and spectral projections for this metallic solution at different values of inverse temperature are shown in Fig. 1. For all the temperatures examined in this short bond length regime, the self-energy displays a Fermi liquid character.

In our previous work³⁸, we observed a small internal energy difference between the solutions obtained using

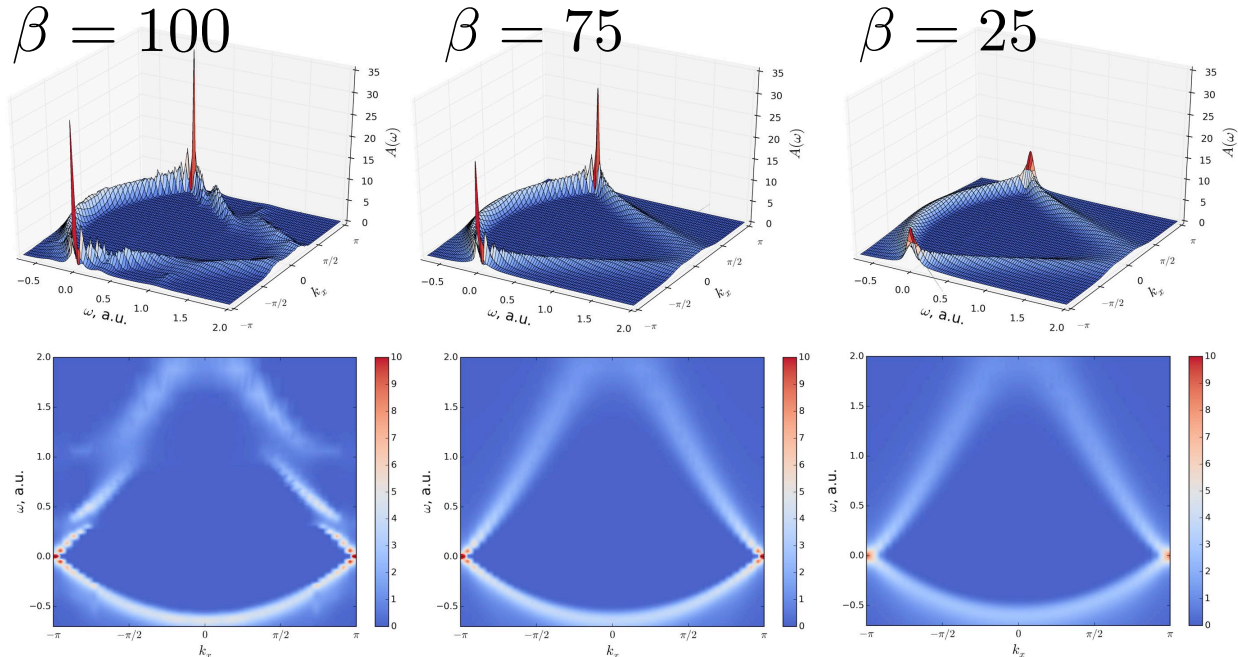


FIG. 1. Spectral functions and projections at different inverse temperatures for the metallic solution at $R=0.75 \text{ \AA}$.

different starting point at $\beta = 100$. We currently observe that this difference can be eliminated if we assure that the convergence criteria are not only fulfilled for the total energy $E_{tot} = E_{1b} + E_{2b}$ but also both the E_{1b} and E_{2b} components separately.

2. Intermediate bond length/intermediate pressure

Spectral functions and projections for the 1D hydrogen solid with an interatomic separation of 1.75 \AA are presented in Fig. 2. We have displayed differences in internal energy (E), entropy (written as $-T\Delta S$), and Helmholtz energy (A) in Table II. For this system at the inverse temperatures of $\beta = 100$ and 75 we obtained two solutions from two different initial guesses. We are able to characterize the first solution (“solution 1”) as a band insulator since the spectral function shows a gap and the self-energy displays a Fermi liquid profile. The second solution (“solution 2”) is gapless and therefore a metal. At an inverse temperature of $\beta = 25$, both “solution 1” and “solution 2” obtained from two different starting guesses have the same spectra and identical Helmholtz energy, indicating that there is only one stable solution — a single phase. Note that in Fig. 2 for $\beta = 25$ both the spectral functions for “solution 1” and “solution 2” seem to have different heights; however, it is an illusion since both spectral functions are plotted with a different z-axis range. We deem that the Helmholtz energy is identical for both these solutions at $\beta = 25$ since the obtained

β	ΔE	$-T \Delta S$	ΔA
100	-0.00370	0.10854	0.10484
75	-0.00528	0.09971	0.09443
25	1.36×10^{-8}	-2.94×10^{-6}	-2.93×10^{-6}

TABLE II. Thermodynamic data for a 1D periodic hydrogen solid with separation $R=1.75 \text{ \AA}$. The units for β are $1/\text{a.u.}$. The units for all other quantities are a.u. All values are obtained by subtracting “solution 1” from “solution 2”. $\Delta E = E_{sol2} - E_{sol1}$, $\Delta A = A_{sol2} - A_{sol1}$, $\Delta S = S_{sol2} - S_{sol1}$. Please note that the quantities at $\beta=25$ are below the precision of convergence (1×10^{-5}).

differences are below our convergence threshold which is 1×10^{-5} a.u.

For two lower temperatures ($\beta = 100$ and 75) by comparing thermodynamic quantities, we are able to determine which phase, “solution 1” or “solution 2”, is the most thermodynamically stable. From the data in Table II, we are able to determine that “solution 1” is the most stable phase from the positive value of ΔA at both $\beta=100$ and $\beta=75$. It is also interesting to note, that this solution is stable due to the entropic factor not due to the difference in the internal energy.

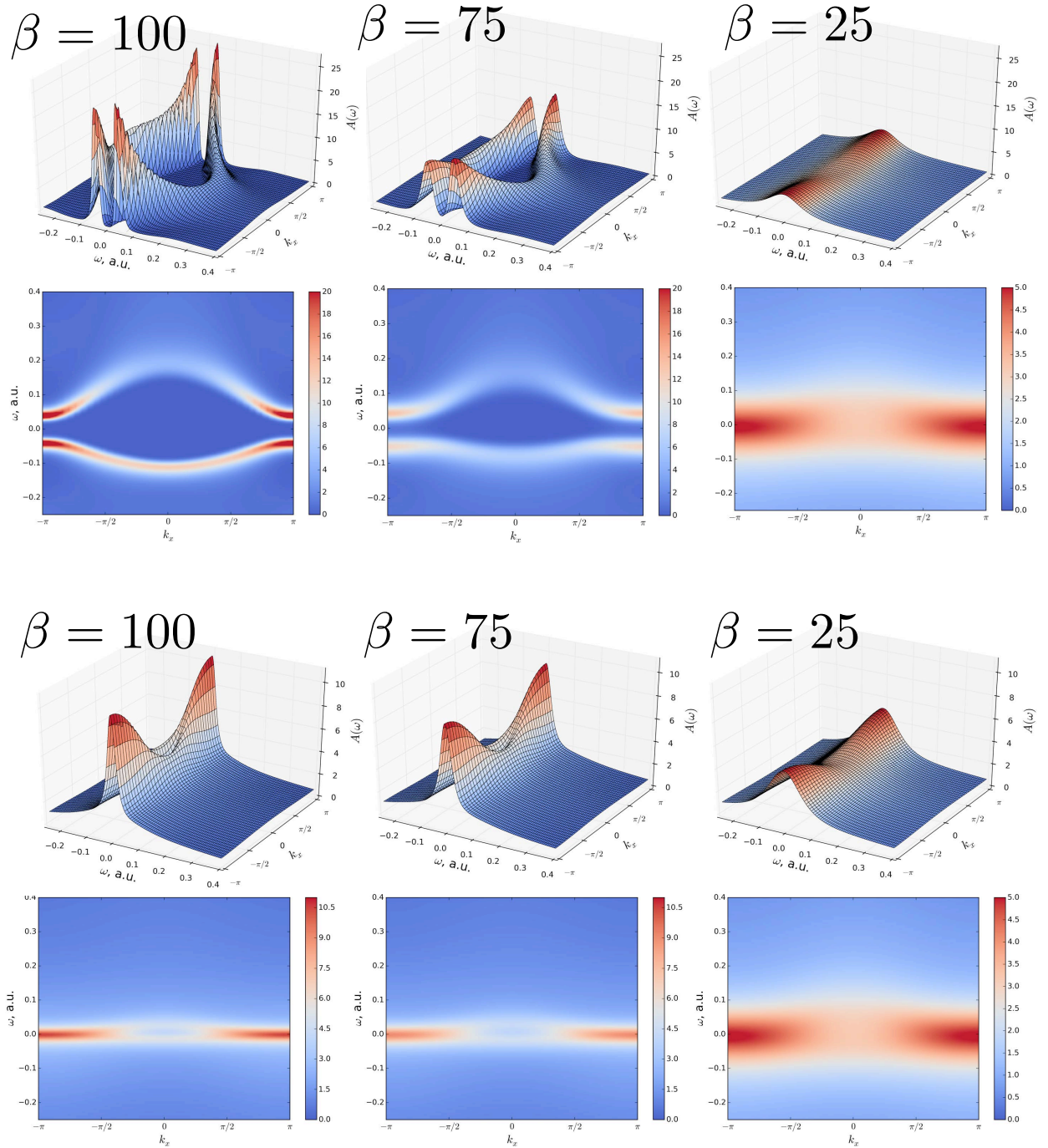


FIG. 2. Spectral functions and projections at different inverse temperatures for the band insulator (“solution 1”) and the metallic solution (“solution 2”) at $R=1.75 \text{ \AA}$. Please note the difference in scale between “solution 1” and “solution 2”.

3. Long bond length/low pressure

Similar to the $R=1.75 \text{ \AA}$ regime, for an interatomic separation of 2.5 \AA at inverse temperatures $\beta = 100$ and 75 , we recover two solutions from the two different ini-

tial guesses, see Fig. 3. At a high temperature $\beta=25$ we observe only one solution independent of the initial guess, and thus only a single phase is present. From the positive value of ΔA we are able to see that “solution 1” is the most stable phase at $\beta=75$ and $\beta=100$ (Ta-

β	ΔE	$-T \Delta S$	ΔA
100	0.08489	0.16257	0.24746
75	0.07103	0.16155	0.23259
25	6.09×10^{-8}	2.96×10^{-5}	2.97×10^{-5}

TABLE III. Thermodynamic data for a 1D periodic hydrogen solid with separation $R=2.5 \text{ \AA}$. The units for β are 1/a.u. The units for all other quantities are a.u. All values are obtained by subtracting “solution 1” from “solution 2”. $\Delta E = E_{sol2} - E_{sol1}$, $\Delta A = A_{sol2} - A_{sol1}$, $\Delta S = S_{sol2} - S_{sol1}$. Please note that the quantities at $\beta=25$ are below or comparable with the precision of convergence (1×10^{-5}).

ble III). This solution is a band insulator since it has a Fermi liquid self-energy profile at these temperatures. The other solution, denoted as “solution 2” at low temperature is metallic and changes into a Mott insulator at high temperatures. The internuclear distance of $R=2.5 \text{ \AA}$ is close to the region where the phase transition occurs, thus results obtained from GF2 which is a low order perturbation expansion may not be reliable. The low level perturbation theories such as GF2 are known to be more accurate deep within a phase and can experience problems near the phase transition point.

Finally, at an interatomic separation of $R=4.0 \text{ \AA}$, for all the temperatures, both initial guesses yield the same converged GF2 result - a single phase. The spectra as a function of inverse temperature can be seen in Fig. 4. This single solution is the Mott insulator as confirmed by the divergent imaginary part of the self-energy.

4. GF2 phase diagram for 1D hydrogen solid

It is instructive now to collect all the data and plot a simple phase diagram for the 1D hydrogen solid as a function of inverse temperature β and intermolecular distance R . We have plotted the phase diagram in Fig. 5. On this diagram, for these regions where two phases coexist, we denoted the most stable phase according to the Helmholtz energy A by framing its symbol using a black line.

For the shortest bond length ($R=0.75 \text{ \AA}$), the 1D hydrogen solid remains metallic at all temperatures considered and only one phase is present.

At intermediate bond lengths ($R=1.75, 2.0 \text{ \AA}$), multiple phases coexist. At lower temperatures, we recover both a metal and band insulator as possible solutions, with the band insulator being the most stable phase according to the Helmholtz energies. This is in line with physical intuition that we should recover an insulator rather than a metal at low temperature. For $R=1.75 \text{ \AA}$, at temperatures higher than $\beta = 50$, we recover only the metallic phase.

For $R=2.0 \text{ \AA}$ at high temperature ($\beta = 25$), we see both a metal and a Mott insulator coexisting, with the Mott insulator being the most stable phase. At lower temperatures, we see the coexistence of a metallic and band insulator solution. The Helmholtz energy indicates that band insulator is the most stable phase.

At a longer bond length of ($R=2.5 \text{ \AA}$), multiple phases are still present. As in the cases of intermediate bond length, we recover both a band insulator and a metal solution, with Helmholtz energy favoring the band solution. We would like to reiterate that a phase transition occurs somewhere in this intermediate region, and it is likely that the results of a second-order perturbation theory may not be accurate enough. At higher temperatures, we recover a Mott insulator as the only phase present.

For the longest bond length ($R=4.0 \text{ \AA}$), the system remains a Mott insulator at all studied temperatures.

VI. CONCLUSION

While the theory describing the connection between the Matsubara Green’s function formalism and thermodynamics has been known since the 1960s, few computational methods are currently capable of employing the Matsubara formalism for realistic systems. This is due to its computationally demanding nature that requires complicated time and frequency grids as well as the iterative nature of the equations.

In our last work³⁸, we have demonstrated one of the first applications of the fully self-consistent Matsubara Green’s function formalism to a realistic periodic problem, that is, a 1D hydrogen solid. In the current work, we have shown that it is possible to evaluate temperature dependent thermodynamic quantities using a self-consistent second-order Green’s function method. Using the self-consistent Green’s function and self-energy, we were able to evaluate the Luttinger-Ward functional at various temperatures and obtain static thermodynamic quantities such as Helmholtz energy, internal energy, and entropy. Evaluation of these quantities gives access to the partition function and any thermodynamic quantity that can be derived from it. Unlike the FCI case, in GF2 we do not need to explicitly calculate excited state energies or Boltzmann factors, making calculation of thermodynamic quantities for larger systems feasible.

To calibrate the thermodynamic data obtained from GF2 against FCI, we have illustrated that for a hydrogen fluoride molecule at high temperature, we are able to obtain energies in excellent agreement with finite temperature FCI. In the lower temperature regime, we observed, as expected, some deviation from the FCI answer but the overall quality of the results still remained high.

Finally, since the thermodynamic data can be used to construct phase diagrams, we used a simple 1D hydrogen solid to investigate possible phases at different temperatures and interatomic distances. We obtained different phases such as a band insulator, Mott insulator, or metal,

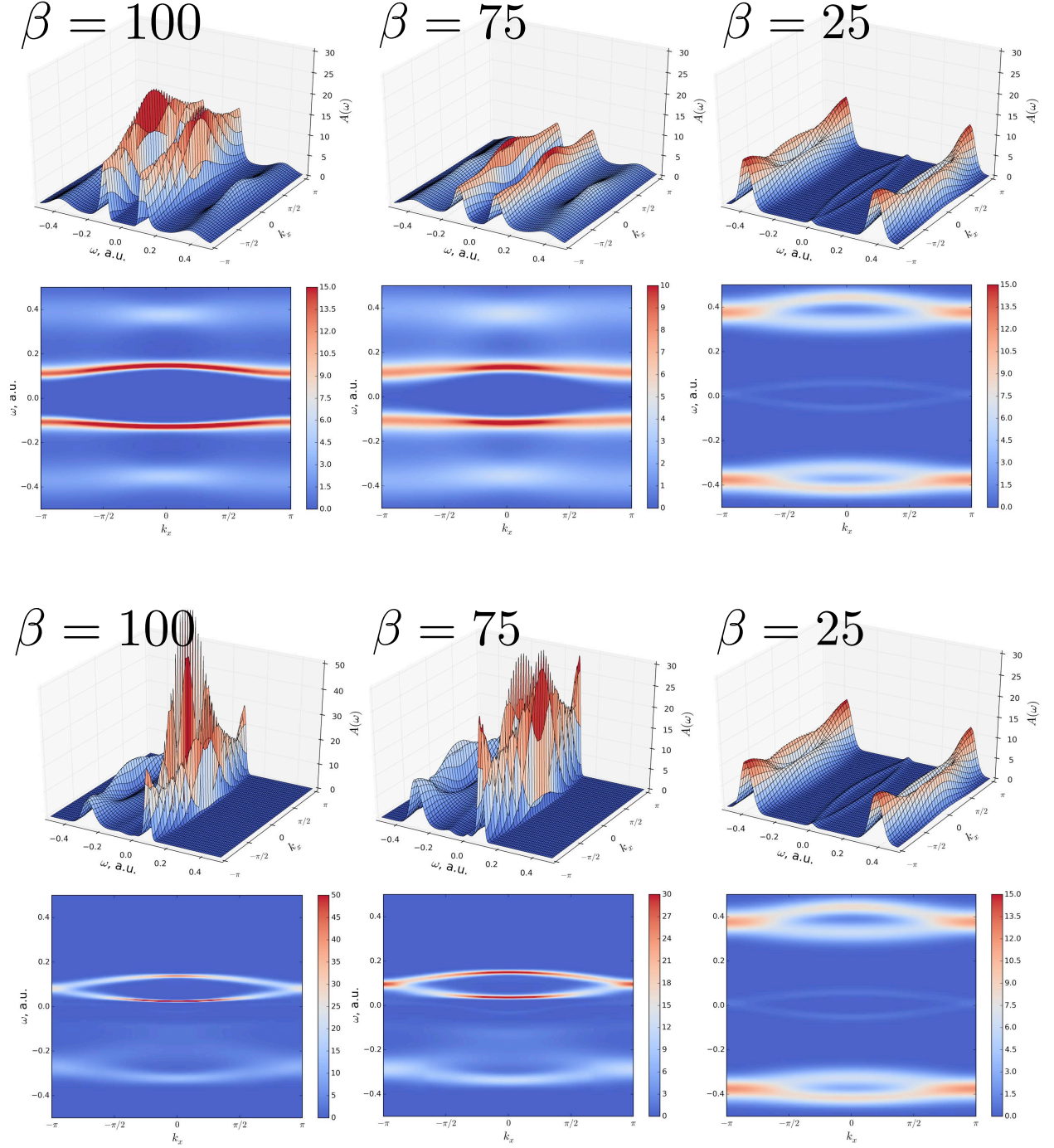


FIG. 3. Spectral functions and projections at different inverse temperatures for the band insulator (“solution 1”) and the metallic solution (“solution 2”) at $R=2.5 \text{ \AA}$.

and we were able to distinguish which phase is more stable at various temperatures. Determining the stability is possible due to our ability to calculate not only the internal energy but also the entropic contribution at each temperature. Consequently, based on the difference of

the Helmholtz energy, we are able to determine the most stable phase for each of the temperature points.

While we acknowledge that GF2 is a low order perturbative method and as such can deliver results that are inaccurate, we believe that for most weakly and mod-

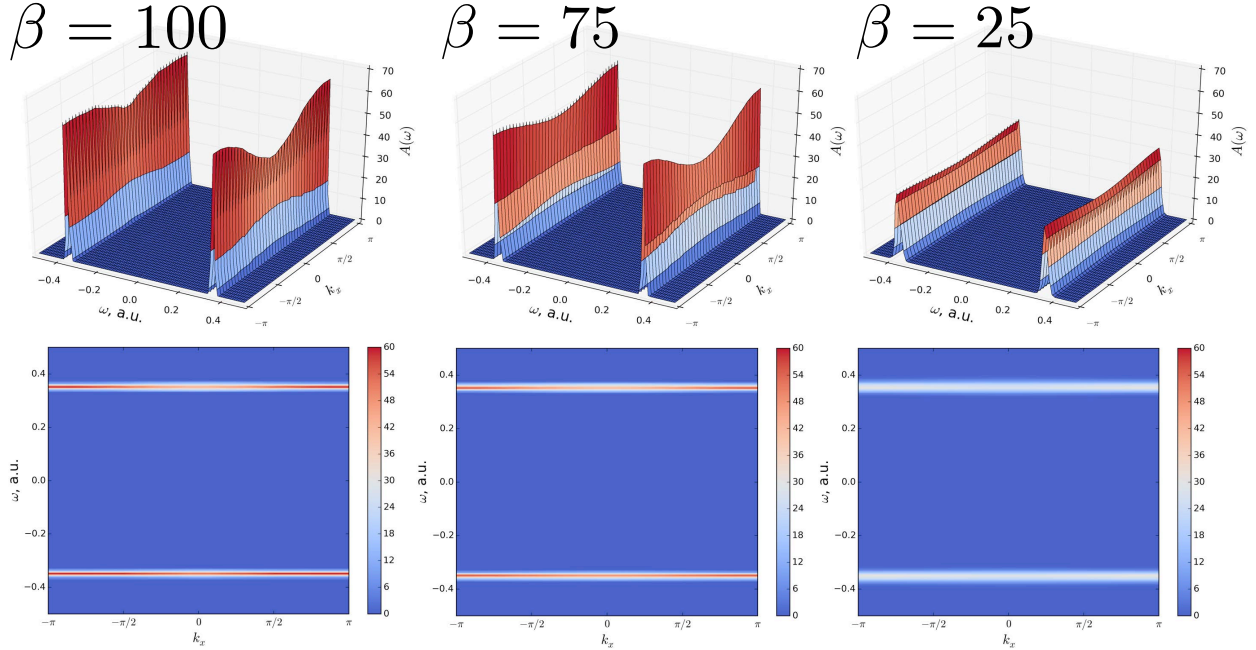


FIG. 4. Spectral functions and projections at different inverse temperatures for the Mott insulator at $R=4.0 \text{ \AA}$.

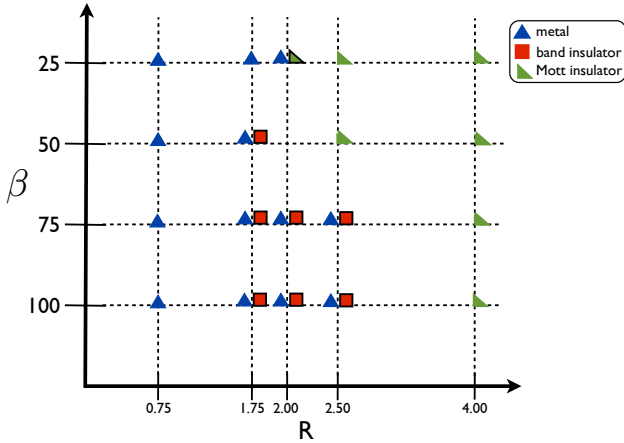


FIG. 5. A phase diagram containing all distances and temperatures calculated for a 1D hydrogen solid. Where multiple phases exist, the most stable phase is outlined in black. β is inverse temperature in units $1/\text{a.u.}$ and R is the separation between hydrogens in \AA .

erately correlated systems such as semiconductors with small band gaps, or alloys, it can be used in the future to provide accurate thermodynamic data and phase diagrams. For systems where the correlations are strong, GF2 can be combined with methods such as self-energy embedding theory (SEET)^{43,44} to provide accurate answers concerning thermodynamics.

ACKNOWLEDGMENTS

D.Z. and A.R.W. would like to acknowledge a National Science Foundation (NSF) grant No. CHE-1453894. A.A.R. acknowledges a Department of Energy (DOE) grant No. ER16391.

VII. APPENDIX: HIGH-FREQUENCY EXPANSION OF THE GREEN'S FUNCTION FOR EVALUATING THE LUTTINGER-WARD FUNCTIONAL

Here, we consider the contribution to the Luttinger-Ward functional in the high frequency limit. In the Matsubara formalism for large frequencies, the Green's function and self-energy can be expressed as a series

$$G(i\omega_n) = \frac{G_1}{i\omega_n} + \frac{G_2}{(i\omega_n)^2} + \mathcal{O}\left(\frac{1}{(i\omega_n)^3}\right) \quad (24)$$

$$\Sigma(i\omega_n) = \frac{\Sigma_1}{i\omega_n} + \frac{\Sigma_2}{(i\omega_n)^2} + \mathcal{O}\left(\frac{1}{(i\omega_n)^3}\right) \quad (25)$$

The coefficients for the Green's function expansion for non-orthogonal orbitals with a quantum chemistry

Hamiltonian⁴⁵ are given as

$$\begin{aligned} G_1 &= S^{-1} \\ G_2 &= S^{-1}(F - \mu S)S^{-1}. \end{aligned} \quad (26)$$

The Σ_1 and Σ_2 coefficient of the self-energy has a complicated explicit form⁴⁵ and is evaluated numerically as

$$\begin{aligned} \Sigma_1 &= \text{Re}(\Sigma(i\omega_{max}) \times i\omega_{max}) \\ \Sigma_2 &= \left(\Sigma(i\omega_{max}) - \frac{\Sigma_1}{i\omega_{max}} \right) \times (i\omega_{max})^2. \end{aligned} \quad (27)$$

For the molecular example in this work, the high frequency contribution to $\text{Tr}[G\Sigma]$ was evaluated as in was done previously^{34,36}. At the very high temperatures considered for the molecule, the high frequency contribution becomes negligible. However, it is necessary to include at the lower temperatures considered. The high-frequency contribution to the $\Omega_{Tr[G\Sigma]}^k$ term of Eq. 19 can be evaluated in a way analogous to the molecular case.

To evaluate the high frequency contribution to the logarithm term $\text{Tr}[\ln\{1 - G\Sigma\}]$ in Eq. 17, we expanded the logarithm as a Taylor series $\ln(1 - x) = x - \frac{x^2}{2} + \dots$ to give

$$\ln\left(1 - \frac{G_1\Sigma_1}{(i\omega_n)^2}\right) = \frac{G_1\Sigma_1}{(i\omega_n)^2} + \mathcal{O}\left(\frac{1}{(i\omega_n)^3}\right). \quad (28)$$

We exclude in this expansion all terms that are equal or lower than $\mathcal{O}\left(\frac{1}{(i\omega_n)^3}\right)$ since they are small. It is only necessary practically to evaluate the first term in the expansion to capture the important contribution from the high frequency limit. We would like to emphasize that although we do not present results including the high frequency contribution to the logarithm term $\text{Tr}[\ln\{1 - G\Sigma\}]$ in Eq. 17 for the periodic hydrogen solid, this term was evaluated and was found to be minuscule compared to the magnitude of the other energies. However, it is possible that this contribution may be substantial for other systems.

-
- * Corresponding author: welden@umich.edu
† Corresponding author: rusakov@umich.edu
‡ Corresponding author: zgid@umich.edu
- ¹ D. A. McQuarrie and J. D. Simon, *Molecular thermodynamics* (University Science Books Sausalito, CA, 1999).
 - ² J. W. Ochterski, Gaussian Inc, Pittsburgh, PA, 1 (2000).
 - ³ J. Y. Tsao, *The World of Compound Semiconductors* (Citeseer).
 - ⁴ E. G. Moroni, G. Grimvall, and T. Jarlborg, *Physical Review Letters* **76**, 2758 (1996).
 - ⁵ T.-Q. Yu and M. E. Tuckerman, *Physical Review Letters* **107**, 015701 (2011).
 - ⁶ Q. Zhu, A. G. Shtukenberg, D. J. Carter, T.-Q. Yu, J. Yang, M. Chen, P. Raiteri, A. R. Oganov, B. Pokroy, I. Polishchuk, *et al.*, *Journal of the American Chemical Society* **138**, 4881 (2016).
 - ⁷ N. D. Mermin, *Annals of Physics* **21**, 99 (1963).
 - ⁸ N. D. Mermin, *Physical Review* **137**, A1441 (1965).
 - ⁹ M. Dharma-wardana, arXiv preprint arXiv:1602.04734 (2016).
 - ¹⁰ J. Smith, A. Pribram-Jones, and K. Burke, arXiv preprint arXiv:1509.03097 (2015).
 - ¹¹ V. V. Karasiev, T. Sjoström, J. Dufty, and S. Trickey, *Physical Review Letters* **112**, 076403 (2014).
 - ¹² S. Hirata and X. He, *The Journal of Chemical Physics* **138**, 204112 (2013).
 - ¹³ M. Altenbökum, K. Emrich, H. Kümmel, and J. Zabolitzky, in *Condensed matter theories* (Springer, 1987) pp. 389–396.
 - ¹⁴ S. H. Mandal, R. Ghosh, G. Sanyal, and D. Mukherjee, *International Journal of Modern Physics B* **17**, 5367 (2003).
 - ¹⁵ M. R. Hermes and S. Hirata, *The Journal of Chemical Physics* **143**, 102818 (2015).
 - ¹⁶ J. Jaklič and P. Prelovšek, *Physical Review B* **49**, 5065 (1994).
 - ¹⁷ J. Prelovšek, P. Bonca, arXiv preprint arXiv:1111.5931 (2011).
 - ¹⁸ G. Stefanucci and R. van Leeuwen, *Nonequilibrium Many-Body Theory of Quantum Systems: A Modern Introduction* (Cambridge University Press, 2013).
 - ¹⁹ R. D. Mattuck, *A Guide to Feynman Diagrams in the Many-Body Problem* (Courier Corporation, 2012).
 - ²⁰ A. L. Fetter and J. D. Walecka, *Quantum theory of many-particle systems* (Courier Corporation, 2003).
 - ²¹ I. Dzyaloshinski *et al.*, *Methods of quantum field theory in statistical physics* (Courier Corporation, 1975).
 - ²² G. Li, W. Hanke, A. N. Rubtsov, S. Båse, and M. Potthoff, *Physical Review B* **80**, 195118 (2009).
 - ²³ M. Potthoff, M. Aichhorn, and C. Dahnken, *Physical Review Letters* **91**, 206402 (2003).
 - ²⁴ M. Potthoff, *The European Physical Journal B-Condensed Matter and Complex Systems* **36**, 335 (2003).
 - ²⁵ M. Potthoff, arXiv:1407.4065 [cond-mat.str-el].
 - ²⁶ M. Potthoff, *The European Physical Journal B-Condensed Matter and Complex Systems* **32**, 429 (2003).
 - ²⁷ W. H. Dickhoff and D. Van Neck, *Many-body theory exposed!: propagator description of quantum mechanics in many-body systems* (World Scientific, 2008).
 - ²⁸ J. M. Luttinger and J. C. Ward, *Physical Review* **118**, 1417 (1960).
 - ²⁹ R. van Leeuwen, N. E. Dahlen, and A. Stan, *Physical Review B* **74**, 195105 (2006).
 - ³⁰ N. E. Dahlen, R. van Leeuwen, and U. von Barth, *Physical Review A* **73**, 012511 (2006).
 - ³¹ C.-O. Almbladh, U. V. Barth, and R. v. Leeuwen, *International Journal of Modern Physics B* **13**, 535 (1999).
 - ³² V. Janiš, *Physical Review B* **60**, 11345 (1999).
 - ³³ V. Janis, *Journal of Physics: Condensed Matter* **15**, L311 (2003).
 - ³⁴ J. J. Phillips and D. Zgid, *The Journal of Chemical Physics*

- 140**, 241101 (2014).
- ³⁵ J. J. Phillips, A. A. Kananenka, and D. Zgid, *The Journal of Chemical Physics* **142**, 194108 (2015).
- ³⁶ A. A. Kananenka, A. R. Welden, T. N. Lan, E. Gull, and D. Zgid, *Journal of Chemical Theory and Computation* (2016).
- ³⁷ A. A. Kananenka, J. J. Phillips, and D. Zgid, *Journal of Chemical Theory and Computation* (2016).
- ³⁸ A. A. Rusakov and D. Zgid, *The Journal of Chemical Physics* **144**, 054106 (2016).
- ³⁹ G. Baym and L. P. Kadanoff, *Physical Review* **124**, 287 (1961).
- ⁴⁰ Z. Kou and S. Hirata, *Theoretical Chemistry Accounts* **133**, 1 (2014).
- ⁴¹ In our molecular calculations we have used 200 Legendre polynomials, 50,000 points on the imaginary frequency grid, and 5,200 imaginary-time points, corresponding to the full grid size before the spline interpolation technique was employed for the imaginary frequency grid. One can expect a reduction to 10% of the original grid size using this technique. We used the most strict criteria for the accuracy, corresponding to a $\delta = 10^{-7}$. Additionally, the Legendre basis vastly reduces the cost arising from the number of τ points on the time grid.
- ⁴² S. Huzinaga, *Gaussian basis sets for molecular calculations* (Elsevier, Amsterdam, 1984).
- ⁴³ A. A. Kananenka, E. Gull, and D. Zgid, *Physical Review B* **91**, 121111 (2015).
- ⁴⁴ T. N. Lan, A. A. Kananenka, and D. Zgid, *The Journal of Chemical Physics* **143**, 241102 (2015).
- ⁴⁵ A. A. Rusakov, J. J. Phillips, and D. Zgid, *The Journal of Chemical Physics* **141**, 194105 (2014).